Pergamon

Int. J. Heat Mass Transfer. Vol. 37, Suppl. 1, pp. 123–132, 1994

0017-9310/94 $6.00 + 0.00

0017-9310(93)0063-M

Multi-phase mixing of liquid cryogens in the simulation of explosion hazards

T. S. LUCHIK, E. Y. KWACK, K. M. AARON, P. SHAKKOTTAI and L. H. BACK
Jet Propulsion Laboratory, California Institute of Technology, Pasadena, CA 91109, U.S.A.

Abstract—Experiments simulating mixing of liquid oxygen (LO_2) and liquid hydrogen (LH_2) have been performed. The non-reactive mixtures were obtained by injecting jets of the oxidizer or simulant into a pool of the fuel or simulant. Three fluid combinations were tested: LO_2 into liquid helium (LHe), liquid nitrogen (LN_2) into LHe and LN_2 into LH_2. Experimental observations included flash X-ray and high speed video imaging, hot film anemometry, and thermocouple and diode thermometry. Results showed that the jet fluid stays coherent throughout the mixing process and that peak boiling of the pool fluid occurs shortly after jet impingement. Estimates of bulk density indicate a smaller range of variation than is currently being used for explosive yield calculations.

1. INTRODUCTION

IN CARRYING out the required Radioisotope Thermoelectric Generator (RTG) hazard definition analysis for several of the Jet Propulsion Laboratory's planetary missions, it became evident that the potential threat to the RTGs from an explosion of liquid oxygen (LO_2) and liquid hydrogen (LH_2) as a result of a launch vehicle accident was not well defined or understood. LH_2 and LO_2 are the propellants for the Space Shuttle and the Centaur G′ upper stage booster. These launch vehicles are used to launch the various JPL spacecraft. The lack of understanding stems from an inadequate data base on close-in blast characteristics for LO_2/LH_2 explosions. The existing data base [1] emphasized far field blast characteristics. However, it is the near field blast environment which impacts RTG safety. An Explosion Hazards Program [2] was initiated to address the near-field effects with special reference to accidental LO_2/LH_2 explosions resulting from a launch vehicle accident.

From an explosion hazards perspective, it is the initial mixing of the LO_2 and LH_2 during which a detonable mixture of multi-phase oxygen and hydrogen is formed. Current predictive techniques assume that the initial blast yield is directly proportional to the bulk-mean density of the mixture. This property, bulk density, is somewhat *ad hoc* since hydrogen and oxygen are immiscible. Nonetheless, it is clear to see that reasonable limits must be placed on this parameter if predictive codes are to be used to obtain realistic estimates of blast yield from full scale simulations.

The study of this problem, even in inert mixtures, presents several difficulties. The mixture is at cryogenic temperatures, it is multi-phase, multi-constituent and is transient in both energy and momentum. The oxidizer is cooled and eventually freezes while the fuel evaporates and is heated. The net result is a harsh environment to make any type of measurements.

Because it was desired to study the mixing of the fuel and oxidizer prior to detonation, simulants for either the fuel or oxidizer were used. Initially tests were performed with LHe as the fuel simulant so that either LN_2 or LO_2 could be used as the oxidizer. This allowed a direct comparison of LN_2 to the real oxidizer, LO_2. Later tests were performed using LH_2 as the fuel. However, only LN_2 could be used as the oxidizer simulant in this case. Thus, performing similar tests with these three inert combinations, allows one to draw conclusions on the mixing of the actual fuel and oxidizer prior to detonation.

Several possible scenarios were considered in explosion hazards investigation. The first of these, the deep mixing scenario, is reported on in this paper. A jet of one fluid is injected into a deep pool of a second fluid in a manner similar to that of the work of Bishop *et al.* [3]. Their tests showed that significant jet penetration occurred only when the more dense fluid (oxidizer simulant) was injected into a pool of the less dense fluid (fuel simulant). When the jet and host fluids were switched very little penetration and mixing occurred. Therefore, in the present study, only the mixing of oxidizer simulants injected into pools of fuel simulants are considered.

2. APPARATUS

This section gives a brief overview of the facility, instrumentation and procedures used in the experiments. For more detailed descriptions see Luchik *et al.* [4, 5]. A schematic of the facility is shown in Fig. 1. The primary enclosure is mainly an exhaust duct for the liquid fuel (or simulant fuel) that is boiled off during an experiment. This enclosure houses all plumbing to the oxidizer tank as well as instrumentation used for thermal and velocity measure-

NOMENCLATURE

c_p	specific heat
h	enthalpy
h_{fg}	heat of vaporization
h_{fs}	heat of fusion
l	liquid penetration distance at time when bulk density was calculated
m	mass
$\dot{m}$	mass flow rate
T_g	gas temperature
u	axial velocity
V_{mix}	mixing volume.

Greek symbols

ρ	density
$\bar{\rho}$	bulk density.

Subscripts

BP	boiling point
FP	freezing point
g	gas value
jet	jet
l	liquid
s	solid.

ments made during an experiment. The stainless steel dump tank used in the experiments is 14.6 cm in diameter and has a capacity of 10.4 l. Flow out of the dump tank was controlled using a pneumatically operated cryogenic ball valve. The flow rate out of the dump tank or injection velocity was controlled by regulating the pressure of the fluid inside the tank. The dewar has a diameter of 14.3 cm and is roughly one meter in length. Located at the top of the primary enclosure, was a 10.2 cm diameter exhaust stack where the fuel evaporation rate was measured. The exhaust gas then flowed into a dilution duct where the exhausted fuel was diluted below its flammability limit and was exhausted to the atmosphere.

As shown in Fig. 1, the primary enclosure was located inside the secondary enclosure which is a small room 3.66 m on a side. The secondary enclosure was purged free of oxygen prior to each experiment and the oxygen level was monitored throughout the experiments using a Teledyne Analytical Systems Model 8000 gas detection system.

A schematic of the primary enclosure, dump tank, experimental dewar and instrumentation is shown in Fig. 2. Chromel–constantan thermocouples (type E) were chosen for these experiments based on arguments presented by Barron [6] and ASTM [7]. Because the experiments performed are transient in nature, the temporal response of the instrumentation is quite important. The size of the thermocouples chosen for the experiments was 76 μm which had a response of about 8 ms (90%). This size was a good compromise between speed and robustness (the experiments were fairly violent and smaller thermocouples did not survive the environment with regularity). Cryodiodes were used in locations where sub-40 K temperatures were expected. The sensitivity of a cryodiode is excellent at low temperatures. However, the diodes have slow response times because of large thermal masses.

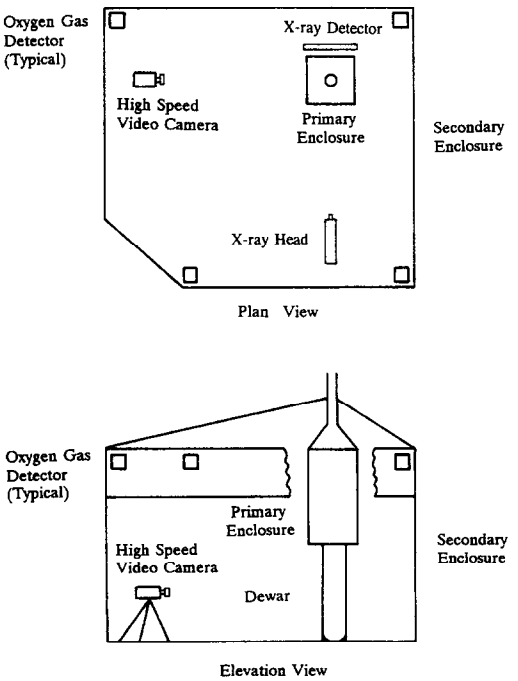

FIG. 1. Facility schematic.

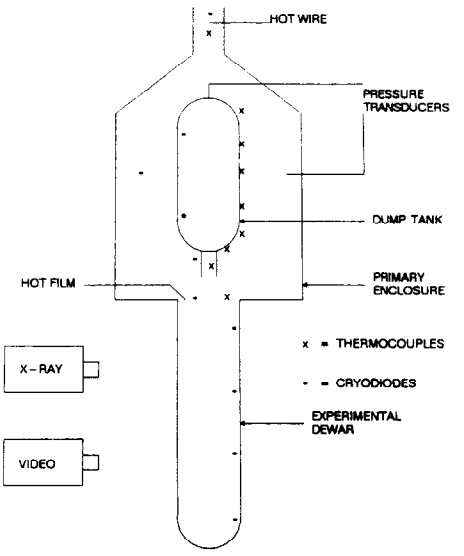

FIG. 2. Schematic of primary enclosure and experimental dewar.

Pressures in the primary and secondary enclosures and in the dump tank were measured using Validyne pressure transducers. Hot film/wire anemometers were used to measure velocities of the fuel boil-off gas at the mouth of the experimental dewar and in the stack of the primary enclosure. However, because of difficulties when helium was used as the fuel simulant, only the stack anemometer yielded useful quantitative information. Although the exhaust stack location offered a less harsh environment than the mouth of the dewar, the measurement was more difficult at the stack since the temperature of the gas at this location varied from 50 K to about 250 K. Thus, a large range of calibration was necessary. The low temperatures tended to destroy hot films after repeated cycling. Details of the hot film/wire calibrations are given in Kwack *et al.* [8] and typical results are shown in Fig. 7 of ref. [9].

A Spin Physics model SP-2000 high speed motion analyzer was used to obtain video recordings of each experiment. For these experiments, recordings were obtained in excess of 500 f.p.s. Typically, the vertical field of view was 45 cm with a minimum spatial resolution of 2.2 mm by 2.2 mm. Data reduction was performed by viewing the images directly at several frames per second and reducing the data manually.

A Hewlett-Packard 300 kV flash X-ray system was used to obtain one X-ray image of the mixing process per experiment with a 50 ns exposure. Each X-ray head has a beryllium window, rather than aluminum, to allow better transmission of the low energy X-rays, which are more sensitive to low molecular weight matter, like LN_2, LO_2, LH_2 and LHe. A wide variety of X-ray receivers were tested in this system. The 'best' receiver tested was the combination of three Dupont products: a Kevlar Cassette with Chronex Quanta Fast Detail screens and either NDT 57 or Chronex 4 film. However, even with this combination, no quantitative results were obtained with the X-ray system. The reason for this is a lack of contrast between the jet and host fluids used in these experiments. However, the X-ray images have yielded valuable information which has been used in developing a qualitative model of the initial mixing during the mixing of the jet and host fluid. It should be noted that the only imaging technique, other than neutron absorption, able to penetrate the mixing zone is the flash X-ray technique.

The data acquisition system was a PC based digital system. The main function of the host during data acquisition is as a memory device for two high speed A/D boards. Data sampling occurred over 23 channels at a rate of 100 scans per second. The A/D board also signaled the host computer at appropriate times to trigger the dump tank operator valve and the flash X-ray system. The host computer controlled the Spin Physics motion analyzer through an RS-232 port.

3. RESULTS

The independent variables for the experiments were the jet velocity, the jet momentum, the dump duration, and the distance between the nozzle exit plane and the free surface of the pool fluid. This distance is referred to as ullage herein. For the various experiments all of the independent variables were varied.

Initially, liquid helium was used as a fuel simulant for the purpose of comparing liquid nitrogen to liquid oxygen. This would prove useful in interpreting the liquid hydrogen/liquid nitrogen experiments. Physical properties of all of the fluids used in the experiments are listed in Table 1. More information on cryogenic fluid properties can be found in Barron [6], Sychev *et al.* [10–12] and Scott [13]. From this table, to a first order approximation, LN_2 appears to be a good simulant for LO_2 in that the thermophysical properties of the fluids are similar. Helium, on the other hand, has one significant property difference from hydrogen, the latent heat of vaporization. This value for helium is approximately a factor of 20 lower for helium than that for hydrogen. Since this property directly affects boiling, the helium evaporation rate cannot be used in any way to approximate hydrogen evaporation.

Varying the nozzle diameter was one way of controlling the mass flow rate of the jet independent of the jet velocity. However the jet diameter played another important role in the experiment. From an X-ray perspective, it was preferable for the jet to be as large in diameter as possible to maximize X-ray contrast between the jet and the host fluid. Fluid dynamically, a small diameter jet is preferable to minimize wall effects. These, of course, are conflicting requirements. Nozzles with diameters of 3.17, 6.34 and 12.7 mm were used in the experiments, but only experiments with the 12.7 mm diameter nozzle yielded useable, qualitative X-radiographs.

3.1. *Helium test results*

Over 70 separate helium experiments were performed where complete data sets were collected, roughly one-half with each jet fluid. The velocity range from 3 to 11 m s^{-1} was covered and ullage was varied from 20 to 76 cm. The purpose of performing tests with helium was to gain some experience in the mixing of two cryogenic fluids in a totally inert environment, but more importantly to determine the similarities and differences in LN_2 and LO_2 as jet fluids. Since later tests would only involve mixing of LN_2 with LH_2, a good working knowledge of this comparison would allow any extrapolation of the present results to the real situation where LO_2 and LH_2 would be involved. Although many tests were run, not all tests were different. Several were similar by design to obtain information on the run to run variation of the experiments. The results of these replicate tests were quite good both qualitatively and quantitatively. An example of this agreement is shown in Fig. 3 for the measured helium gas mass flow rate at the stack, the parameter most sensitive to run to run variations. In this figure, the jet velocity is 3.5 m s^{-1}, the nozzle diameter is 6.35 mm and the dump duration is 0.45 s.

Temporal contours of the mixing zone are shown

Table 1. Some properties of helium, hydrogen, nitrogen and oxygen

	Helium	Hydrogen	Nitrogen	Oxygen
T_{BP} (K) (1 atm)	4.2	20.26	77.35	90.18
T_{FP} (K) (1 atm)	—	13.8	63.15	54.36
ρ_{BP_l} (kg m^{-3})	125	70	807	1141
ρ_{BP_v} (kg m^{-3})	17	1.3	4.6	4.5
h_{fg} (kJ kg^{-1})	21	454	199	213
h_{fs} (kJ kg^{-1})	—	—	25.1	13.8
$h_{\gamma\beta}$ (kJ kg^{-1})	—	—	—	23.4
$T_{\gamma\beta}$ (K)	—	—	—	43.8
$h_{\beta\alpha}$ (kJ kg^{-1})	—	—	~8.4	2.9
$T_{\beta\alpha}$ (K)	—	—	35.6	23.6
$c_{P_{gBP}}$ (kJ kg^{-1} K^{-1})	5.40	12.15	4.73	1.0
$c_{P_{lBP}}$ (kJ kg^{-1} K^{-1})	4.98	9.66	2.13	1.67
$c_{P_{sFP}}$ (kJ kg^{-1} K^{-1})	—	—	1.88	1.42

in Fig. 4 for an LN_2/LHe experiment and an LO_2/LHe experiment. Each of these experiments was nominally

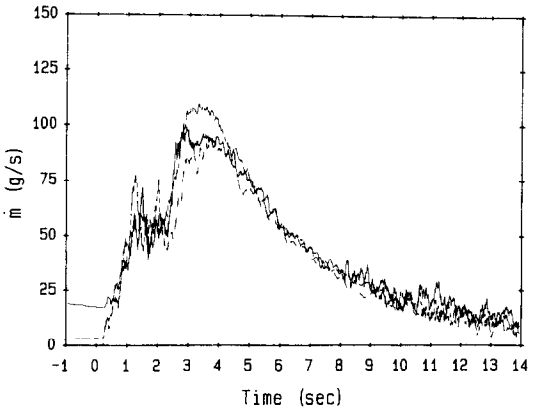

FIG. 3. Helium evaporation rate for three similar tests.

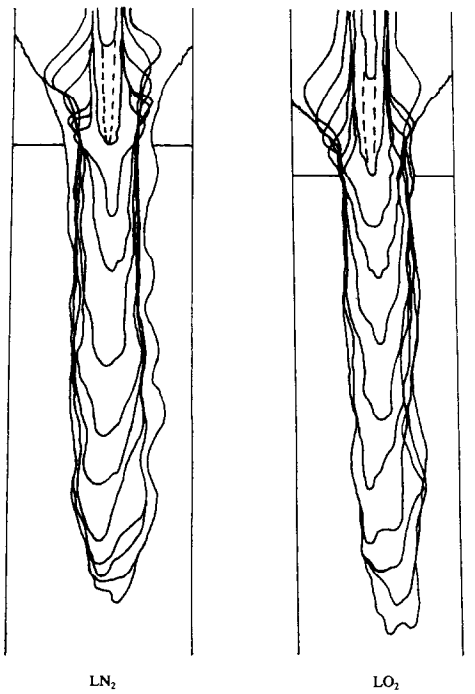

FIG. 4. Mixing zone contours for LO_2 and LN_2 jets into LHe.

at the same conditions, a jet velocity of 3.2 m s^{-1}, 6.35 mm nozzle and 22 cm ullage, with only the jet fluid being different. The solid contours are 'mixing zone' contours at 20 ms time increments while the dashed contour at time $t = 0$ is the estimated liquid 'jet' contour. This estimate of the actual jet fluid location is based on experiments with a LN_2 jet into cold helium gas ($T < 20$ K) and from X-ray observations. From those experiments involving the LN_2 jet into cold He gas it was seen that a mixing zone formed between the relatively warm jet fluid and cold He gas. From this knowledge, we see that prior to impingement of the liquid jet on the helium free surface, a mixing zone is formed. This figure is another example of excellent agreement between the LN_2 and LO_2 jet studies.

The results of the LN_2 tests and the LO_2 tests agreed well in almost every way with one exception—the size of the frozen particle differed. It was noted from the experiments that the solid particles become visually observable at the head of the jet initially and a short time later at the outer most extremity of the mixing zone generally near the region of the initial jet impingement. The particles are first seen about 200–400 ms after jet impingement for all tests, and this time does not vary systematically with any of the independent variables nor with the jet fluid. As observed from the motion of the particles in the case of the LN_2 jet, they are platelet in shape and fall through the liquid helium at a velocity of about 1 m s^{-1}. Quantitative information obtained, based on a sample of 500 particles, indicate that the average size of a particle is 38 mm^2 with sizes ranging from 4 to 130 mm^2, and in general the platelets are less than 1 mm thick. The particles in the case of the LO_2 jet were smaller than those of the LN_2 jet and were generally smaller than the resolution of the video system used. However, large particles could be visualized occasionally. Although no mean size data were obtained for O_2, it was noted that the large O_2 particles were also platelet shaped.

The solids seen in all of the experiments were much larger than is predicted from instability theory, which predicts droplet sizes of the order of microns. Thus,

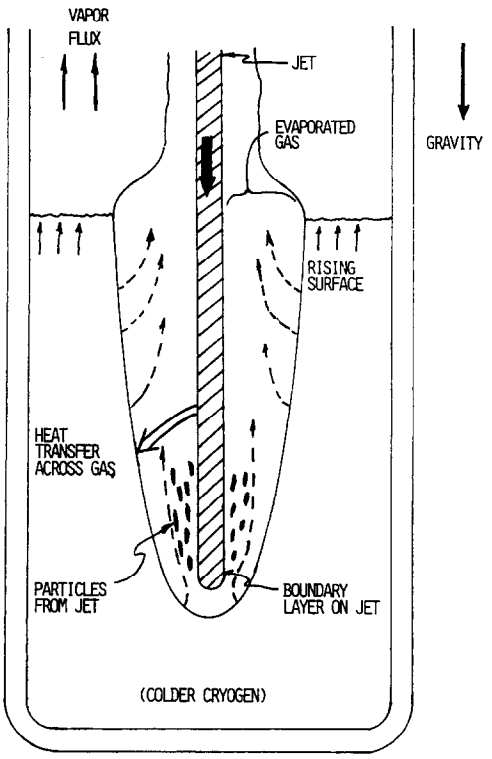

FIG. 5. General mixing zone characteristics.

measurements of particle size would indicate that freezing is occurring at the jet outer extremity while the jet is still intact which agrees with the X-ray images that show that the jet is largely coherent during the mixing process. However, this hypothesis was impossible to verify experimentally since the mixing bubble cannot be penetrated with enough spatial resolution and dynamic range to visualize the actual solidification process. The smallest particles discernable, because of the pixel resolution of the video system, were 4 mm^2 for most of the tests, but as small as 1 mm^2 in some cases.

3.2. *Hydrogen test results*

For the hydrogen tests as in the helium tests, several tests at similar conditions were performed to determine the run-to-run variation of the tests. As was seen in the helium tests, the duplicate experiments yielded similar results.

Figure 5 shows some of the general mixing dynamics for the experimental configuration obtained from the hydrogen tests. The jet impinges on the host fluid which causes boiling of the host and cooling to the eventual freezing point of the jet. As the jet continues to penetrate, a mixing pocket forms which contains some mixture of the gas and liquid state of the host and liquid and solid state of the jet. As time progresses, the fluids within the mixing pocket transfer enough heat between each other so that some freezing of the jet occurs while the host continues to boil off. During the initial mixing of the jet and host fluid the mixing zone is optically too dense to penetrate using conventional optics. However, the radiographs have shown that the jet fluid essentially stays intact and has a diameter approximately equal to that when it leaves the nozzle. Figure 6 shows the mixing zone developed by a 12.7 mm jet of LO_2 with an impingement velocity of 3.2 m s^{-1} into LHe approximately 0.2 s after jet impingement. (A radiograph of an LO_2 jet into liquid helium is shown in Fig. 6 because the radiographs obtained from the hydrogen tests were not of publication quality, although they did contain the same information as the radiograph shown.) The mixing zone contains both jet and host fluid in its liquid state as well as vaporized host. A comparison of visual images to the radiographs showed that the mixing zone is roughly 5–8 times the diameter of the jet. The X-radiographs show further that within the mixing zone the host is largely gas on a volume basis. Somewhat later in the mixing process (about 200–400 ms) solidification of the jet occurs at the head of the jet and near the point of initial impingement.

Mixing zone contours obtained from images taken with the Spin Physics motion analyzer are shown in Fig. 7. These images were obtained for a 3.05 m s^{-1} jet of LN_2 into a pool of hydrogen. The nozzle diameter in this experiment was 12.7 mm. Each contour represents an instant in time and the contours are separated in time by 20 ms. As in Fig. 4, the jet contour at impingement has been shown by a dashed line and was determined in a similar manner to that of Fig. 4. Immediately after impingement, the jet velocity is significantly decreased from its initial velocity. The velocity is less for smaller diameter jets. Figure 8 shows the variation of an average of the jet penetration speed with nozzle size and time. A second surge generates a mixing zone that appears similar to the initial mixing zone. As with the helium studies, very little can be said on the radial rate of formation of the mixing zone other than it does develop more slowly radially than axially.

From the mixing zone impingement contours and from the Spin Physics video in general, several pieces of information were obtained. These include an estimate of the bulk or mean density within the mixing zone, and information on the solidification of the jet fluid. Luchik *et al.* [5, 9] have shown that an upper estimate for bulk density is obtained using

$$\bar{\rho} = \rho_{GH_2} + \frac{\dot{m}_{jet}\Delta t}{V_{mix}}\left(1 - \frac{\rho_{GH_2}}{\rho_{jet}}\right). \quad (1)$$

Here $\dot{m}_{jet}$ is the mass flow rate of jet into the mixing zone and V_{mix} is the volume of the mixing zone at Δt seconds after impingement. In this analysis it is assumed that the mixing zone is axially symmetric, that all of the jet fluid in the mixing zone is in its liquid state while all of the host fluid is in the gaseous state. This is an upper estimate since all of the jet fluid is assumed to be participating in the heat transfer involved in boiling the host fluid. Table 2 shows the

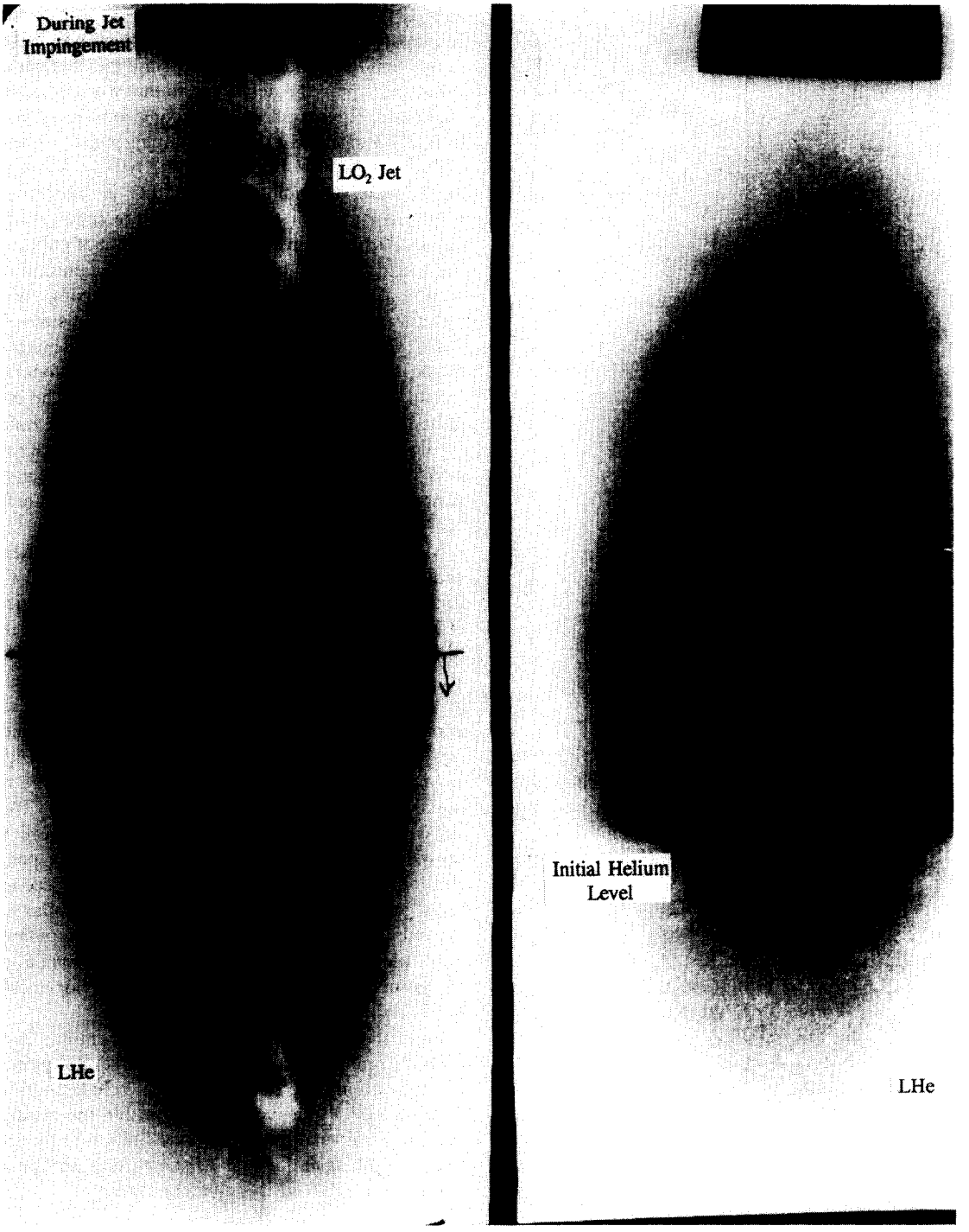

FIG. 6. Radiograph of LO_2 jet into LHe pool.

average values of the upper estimate of bulk density within the mixing zone at early times after impingement obtained from the various experiments. All averages were obtained from mixing zone contours 120 ms after impingement of the jet. For comparison the density of hydrogen vapor at 20.3 K is 0.0013 g cm^{-3}. The estimated values for an oxygen jet were made simply by assuming that the volume occupied by the LN_2 had the density of LO_2 at its normal boiling point. These results are consistent with what was experimentally found in the helium tests [9].

This estimated bulk density does vary with the radius of the jet, a result seen in the helium tests. As is shown in Luchik *et al.* [5], a simple argument can show this to be the expected case which yields

$$\frac{\bar{\rho}-\rho_{GH_2}}{\rho_{jet}-\rho_{GH_2}} \propto \frac{u_{jet}\Delta t}{l}\frac{r_{jet}^2}{r_{jet}} \approx C_1 r_{jet}. \tag{2}$$

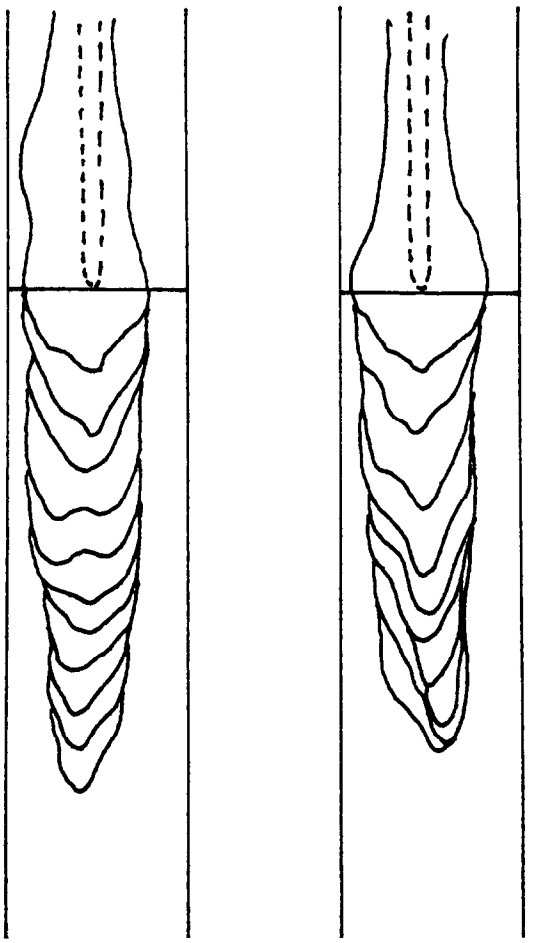

FIG. 7. Mixing zone contours for LN_2 jet into LH_2.

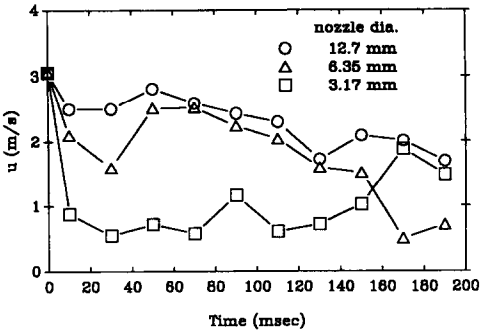

FIG. 8. LN_2 jet penetration velocity after impingement into LH_2.

A second method, which estimates the minimum bulk density can be made from knowledge that the jet remains largely intact in the mixing zone. This indicates that only a portion of the original jet fluid is taking part in the heat transfer required to boil the hydrogen. The analysis is identical to that in Luchik *et al.* [5] except that H_2 has been substituted for He. The result is the following equation:

$$\bar{\rho}_{\min} = \rho_{GH_2}\left(1 + \frac{h_{fg,H_2}}{\Delta h_{jet,max}}\right). \quad (3)$$

The maximum enthalpy change in the jet fluid is achieved by cooling it to the liquid pool temperature (20.3 K for liquid hydrogen). $\Delta h_{jet,max}$ has the value of 124 kJ kg^{-1} for N_2 and 136 kJ kg^{-1} for O_2. Doing this assumes that the minimum jet mass is involved in the heat transfer required for boiling heat transfer, thus yielding the minimum bulk density. Substituting the values for the thermophysical properties gives $\bar{\rho}_{\min} = 0.0059$ g cm^{-3} for LN_2 jets and $\bar{\rho}_{\min} = 0.0055$ g cm^{-3} for LO_2 jets. These values are roughly a factor of two lower than the upper estimate values obtained for the 3.17 mm diameter nozzle indicating that even with that small nozzle size only about one-half of the jet was participating in the heat transfer to the hydrogen. These results are significant in that current predictive techniques cover a range of bulk densities with an upper limit more than one order of magnitude greater than the maximum values presented here.

The size of most of the solid particles in these experiments varied from 7 to 70 mm^2 with the largest particle seen being 350 mm^2. The particles in the hydrogen tests appeared platelet in shape. The size information for the N_2 particles as well as the shape is consistent with what had been seen in the helium tests with a LN_2 jet. The particle size was observed to increase as the jet diameter was increased. Particle information for N_2 was found to be independent of the pool fluid with which it was mixed. This leads to the conclusion that SO_2 particles generated in a mix of LO_2/LH_2 would be similar to those in the LO_2/LHe tests.

The instantaneous temperature of the H_2 gas at the mouth of the dewar and the instantaneous evaporation rate of H_2 are presented in Fig. 9. Results from three different experiments are shown to indicate the consistency from experiment-to-experiment. Nominal conditions for these experiments are a 12.7 mm diameter jet of N_2 flowing with jet velocity of 3.5 m s^{-1} for a period of 0.65 s. In all cases the ullage was roughly 42 cm. Note that impingement of the jet occurs about 0.24 s after the dump valve has been energized ($t = 0$) and that the gas temperature prior to mixing is 70–100 K due to heat transfer from the surroundings. As the rate of evaporation increases,

Table 2. Bulk density estimates during initial jet impingement into LH_2

Jet velocity (m s^{-1})	Nozzle dia. (mm)	LN_2 jet $\bar{\rho}$ (g cm^{-3})	LO_2 jet $\bar{\rho}$ (estimated) (g cm^{-3})
3.0–5.0	3.17	0.013	0.015
3.0–5.0	6.35	0.014±0.006	0.018
3.0–5.0	12.7	0.023±0.009	0.032

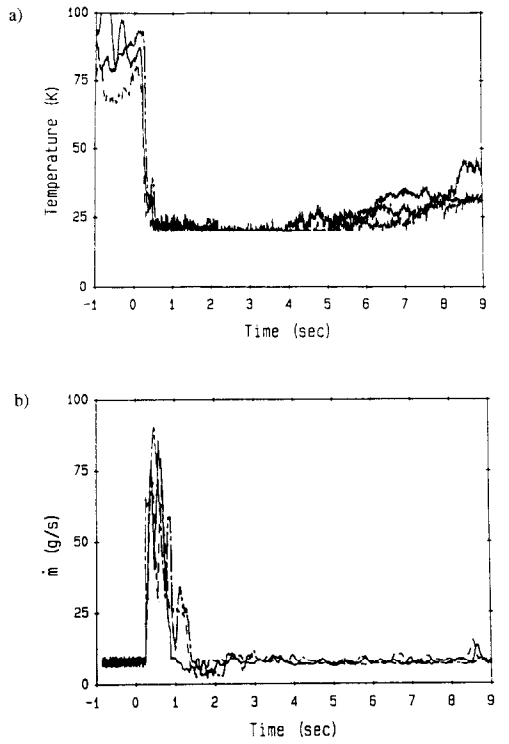

FIG. 9. (a) Mouth temperature variation for three similar tests of LN_2 jet into LH_2 and (b) mass flow rate at mouth of dewar for three similar tests of LN_2 jet into LH_2.

the gas exits the dewar without exchanging heat because the gas residence time in the dewar has decreased. The 'peak and valley' nature of the data shown is believed to be related to the surging of jet fluid in the mixing region seen in the video images. Although not shown, the time at which peak boil off occurred did not vary appreciably. The value of peak boil off was found to vary with the nozzle diameter for a given jet velocity. This result suggests that a principle parameter in the early mixing is the diameter of the jet. More work is needed to verify this trend.

Integrated values of the hydrogen boiled off from a visual displacement measurement along with some representative data taken from the hot-film at the mouth of the experimental dewar are given in Table 3. The purpose of this is to show the accuracy of the hot-film data. Individual values of the ratio of hydrogen boiled off to jet fluid added varied from 0.16 to 0.26.

Table 3. Comparison of time integrated hot film data and hydrogen boil off displacement measurement

Run	$\dot{m}_{jet}$ (g s^{-1})	Δm_{jet} (g)	Δm_{LH_2} (g)	$\Delta m_{GH_2,HF}$ (g)	$\Delta m_{GH_2,HF}/\Delta m_{jet}$
663	306	138	23	25.1	0.18
664	306	199	40	40.8	0.21
665	306	199	37	39.6	0.20
666	306	199	44	41.9	0.21

Table 4. Equilibrium calculation of the ratio of liquid hydrogen vaporized to liquid nitrogen or liquid oxygen solidified

$T_{GH_2,Final} - T_{BP,H_2}$	$\Delta m_{GH_2}/\Delta m_{LN_2}$	$\Delta m_{GH_2}/\Delta m_{LO_2}$
0.0	0.27	0.30
5.0	0.24	0.26
10.0	0.22	0.24
15.0	0.19	0.21
20.0	0.18	0.20
25.0	0.16	0.18

The values obtained are reasonable and can be shown analytically by assuming that a small amount of jet fluid is dumped into a large container of LH_2 and that the final equilibrium temperature of the nitrogen in the hydrogen bath is 20.3 K, then we can develop the relationships (see Luchik *et al.* [4] for derivation)

$$\frac{\Delta m_{H_2}}{\Delta m_{jet}} = \frac{\Delta h_{jet,max}}{h_{fg,H_2} + c_{p,GH_2}(T_{GH_2,Final} - T_{BP,H_2})} \quad (4)$$

where c_p is the specific heat, h_{fg} is the latent heat of vaporization, T is temperature and the subscripts H_2 and jet refer to the given constituent. $\Delta h_{jet,max}$ represents the energy release from the jet fluid when cooled to 20.3 K. Assuming that the hydrogen boils off and leaves the control volume at its boiling point, one can obtain the maximum ratios of hydrogen boiled to jet fluid added. These values are 0.27 and 0.30 for N_2 and O_2, respectively.

However, if the hydrogen gas leaving the control volume is allowed to exchange heat with the jet fluid, the mass ratios can be less than the maximum. Since hydrogen has a high heat of vaporization (454 kJ kg^{-1}) and a relatively low specific heat the variation of boil off with gas exit temperature is small. The boiling of hydrogen occurs at 20.3 K but the temperature that hydrogen leaves the control volume can be higher than that because of heat transfer from either the liquid jet fluid or the relatively warm solid particles to the gaseous hydrogen. Table 4 summarizes the results obtained from equation (4) for both LO_2 and LN_2. Using an average boil-off ratio of 0.2 (from Table 3), Table 4 shows that the average temperature of the hydrogen gas exiting the experimental dewar was 13 K warmer than its normal boiling point. However, the thermocouple at the mouth of the dewar only indicated a superheat of about 5 K during active boiling. The reason for this is probably the lack of resolution of the thermocouples at low temperatures. This implies that between 73 and 88% of the jet fluid energy went into the actual vaporization of the hydrogen liquid pool, on average.

4. SUMMARY

Deep pool mixing studies of LN_2/LHe, LO_2/LHe and LN_2/LH_2 have been conducted. The present mixing studies included varying jet velocities, jet dump duration times, jet diameter and ullage spaces. However, the qualitative nature of the mixing zone does not seem to be greatly affected by these variables although the rate of formation of the mixing zone occurs more rapidly when LHe is the pool fluid than when LH_2 is the pool fluid. Heat exchange between the liquid jet and the colder gas in the ullage space seems to have little effect on the dynamics of the liquid–liquid interaction.

The experiments with LO_2 and LN_2 as the jet fluids showed that N_2 was an excellent simulant for O_2 in all respects except one. The one aspect where N_2 differed from O_2 was in the formation of solid particles. All of the particles observed in the experiments were similar in shape. The motion of these particles in the high-speed video recordings indicated that the particles were platelet in shape. However, in the helium studies, a large number of particles were visualized when LN_2 was the jet fluid whereas when LO_2 was the jet, far fewer particles were clearly visualized. It is believed that the O_2 particles were present, but were too small to be seen with the resolution of the camera system. The solid particles for the N_2 jet were the same size and shape regardless of the pool fluid into which the LN_2 was injected.

The axial rate of formation of the mixing zone slowed with time after impingement of the jet with the formation nearly stopping 150–200 ms after jet impingement. Some 50–150 ms passed before a second surge of jet fluid was seen. The radial rate of formation of the mixing zone was very slow. Maximum boiling of the hydrogen pool occurred 200–300 ms after jet impingement and the value of the maximum boil off rate scaled with the nozzle diameter for a given jet velocity. This indicates that the maximum boil off rate was heavily dependent on the surface area of the jet (i.e. the jet could be modeled as a column of fluid submerged in a pool of hydrogen). This further indicates that the amount of jet fluid sheared from the jet is small. This is further evidenced by the large discrepancies in the maximum and minimum bulk densities and the results of the flash radiographs.

Two different values were obtained for bulk density. One assumed that all of the jet fluid was involved in the heat transfer required to vaporize the hydrogen in the mixing volume. This estimate is a maximum estimate for bulk density since all other indicators show that the entire jet mass is not diffused throughout the mixing zone. The second estimate for bulk density was based on heat transfer concepts. It assumed that the minimum jet mass transferred all of the available energy to the hydrogen and that this energy was used for vaporization only. This estimate is, by definition, the minimum bulk density in the mixing zone allowed by the physics of the problem. The values determined as the upper limit on bulk density for a liquid nitrogen jet into a pool of hydrogen varied with the nozzle diameter and had values ranging from 0.013 g cm^{-3} for the 3.17 mm nozzle to 0.023 g cm^{-3} for the 12.7 mm nozzle. Values for $\bar{\rho}$ were then estimated for LO_2 jets into LH_2. These values were only slightly higher than those for LN_2. The minimum value of bulk density, as determined by analysis, for a LO_2/LH_2 mixture was $\bar{\rho}_{min} = 0.0055$ g cm^{-3}. This range of experimentally/analytically determined values is significantly lower than the estimates being used in predictive detonation environment techniques which use upper limit values as high as $\bar{\rho} = 0.4$ g cm^{-3}.

The shallow mixing experiments were conducted to investigate the influence of the bottom wall of a dewar (spilled mode) and reported elsewhere [14].

Acknowledgements—The work described in this paper was carried out in the Applied Mechanics Technologies Section of the Jet Propulsion Laboratory, California Institute of Technology, under Contract with the National Aeronautics and Space Administration. The assistance of Wayne Bixler and Stan Kikkert throughout this continuing work is acknowledged.

REFERENCES

1. A. B. Willoughby, C. Wilton and J. Mansfield, Liquid propellant explosive hazards, Final Report, AFRPL TR-68-92, URS Research Company (1968).
2. P. F. Massier, J. W. Marshall and R. M. Clayton, Liquid hydrogen/liquid oxygen explosion hazards program plan, JPL D-5113, Internal Document, Jet Propulsion Laboratory, Pasadena, CA (1988).
3. C. V. Bishop, F. J. Benz and L. J. Ullian, Mixing of cryogenic fluids and predicted detonation properties for multi-phase liquid oxygen and liquid hydrogen, presented at the *1986 JANNAF Propulsion Meeting* (1986).
4. T. S. Luchik, K. M. Aaron, G. Fabris, R. M. Clayton and L. H. Back, Cryogenic mixing processes in the simulation of LO_2/LH_2 explosion hazards: experimental facility and initial results with LN_2/LHe, JPL D-6394, Internal Document, Jet Propulsion Laboratory, Pasadena, CA (1989).
5. T. S. Luchik, K. M. Aaron, E. Y. Kwack, P. Shakkottai, R. M. Clayton and L. H. Back, Cryogenic mixing processes in the simulation of LO_2/LH_2 explosion hazards: results with LN_2/LHe and LO_2/LHe, JPL D-6987, Internal Document, Jet Propulsion Laboratory, Pasadena, CA (1990).
6. R. F. Barron, *Cryogenic Systems* (*Monographs on Cryogenics*), pp. 13–58. Oxford University Press, New York (1985).
7. *Manual on the Use of Thermocouples in Temperature Measurements*, ASTM special publication 470A. American Society for Testing and Materials, Philadelphia (1974).
8. E. Y. Kwack, P. Shakkottai, T. S. Luchik, K. M. Aaron, G. Fabris and L. H. Back, Hot-wires/films behavior in low temperature gases, *J. Heat Transfer* **114**, 859–865 (1992).
9. T. S. Luchik, K. M. Aaron, E. Y. Kwack, P. Shakkottai and L. H. Back, Cryogenic mixing processes with phase change in the simulation of LO_2/LH_2 explosion hazards, *Proceedings of 9th International Heat Transfer Conference*, Vol. 1, pp. 365–382. Hemisphere, New York (1990).

10. V. V Sychev, A. A. Vasserman, A. D. Kozlov, G. A. Spiridonov and V. A. Tsymarny, *Thermodynamic Properties of Nitrogen*. Hemisphere, New York (1987).
11. V. V. Sychev, A. A Vasserman, A. D. Kozlov, G. A. Spiridonov and V. A. Tsymarny, *Thermodynamic Properties of Oxygen*. Hemisphere, New York (1987).
12. V. V Sychev, A. A Vasserman, A. D. Kozlov, G. A. Spiridonov and V. A. Tsymarny, *Thermodynamic Properties of Helium*. Hemisphere, New York (1987).
13. R. B. Scott, *Cryogenic Engineering*. Van Nostrand, Princeton, NJ (1959).
14. E. Y. Kwack, T. S. Luchik and L. H. Back, Cryogenic mixing with phase change in the simulation of LO_2/LH_2 explosion hazards: shallow mixing mode, submitted to *Int. J. Heat Mass Transfer*.